

Planar Frequency Selective Bolometric Array at 350 GHz

Sumedh Mahashabde, Alexander S. Sobolev, Mikhail A. Tarasov, Gombo E. Tsydynzhapov, and Leonid S. Kuzmin

Abstract—In this paper, we describe a bolometric focal plane array consisting of the cold electron bolometer (CEB) integrated in a frequency selective surface (FSS) fabricated on a silicon substrate with a backshort. This array is formed by a periodic pattern of conducting annular square and ring shapes and the two-terminal CEB is embedded directly in the element. The impedance of the CEB has been matched to the FSS which provides resonant interaction with incident sub-millimetre radiation. A further degree-of-freedom for the tuning is via varying the thickness of the substrate. We have been able to design the FSS at 350 GHz with peak coupling of more than 90% as is common for FSS based filters. A prototype of such a detector has been fabricated and optical response to black-body radiation has been measured, indicating responsivities of $2 * 10^9$ V/W and higher at 185 mK and $3 * 10^8$ V/W and higher at 300 mK. The details of this new concept, together with numerical simulations and optical measurements are presented.

Index Terms—Cold-electron bolometers (CEBs), frequency selective surfaces (FSS), planar detector array, sub-mm wave detectors.

I. INTRODUCTION

THE concept of cold electron bolometers (CEBs) [1] has been developed and recently brought to the level of potential applications for studies of cosmic microwave background, such as BOOMERanG [2], OLIMPO [3], and LSPE [4]. A CEB embedded into an antenna has high responsivity and a small absorber cross section that reduces its sensitivity to high-energy cosmic rays [5] and makes CEBs advantageous for balloon-borne and space-borne missions. The CEB consists of a normal absorbing volume coupled to superconducting electrodes via two SIN tunnel junctions. The SIN junction capacitance allows coupling of high frequency currents excited on the antennae

(or FSS) to the absorber. The SIN junctions also work as electron coolers which improve the device responsivity and their dynamic impedance can be matched to various readout amplifiers. In the process of designing an array of CEB detectors on a substrate, the problem of substrate modes becomes apparent. In order to get rid of substrate resonances [6], submillimeter planar antennas are either integrated with a quasi-optical lens together with the substrate or fabricated on a membrane, whose thickness is less than a quarter of the wavelength. Recently described lumped element kinetic inductance detectors (LEKIDs) operate on a $\frac{3}{4}$ wavelength substrate with an antireflection coating [7]. The effective sheet impedance of periodically arranged LEKID stripes is tuned to that of the free space and does not depend on frequency. As a result, substrate modes do not propagate due to strong absorption in the impedance-matched layer of detectors. This concept of a 2-D imaging array allows filling of the focal plane of a telescope with a large number of detectors, avoiding the use of quasi-optical filters and coupling to incident submillimetre radiation from a wide area determined by the size of Airy spot.

Bolometers due to their nature are sensitive to optical radiation in a wide frequency band. A combination of planar quasi-optical filters based on Frequency Selective Surfaces (FSS) is used to narrow down the bandwidth of incident optical power. These filters are based on a periodically repeating elementary pattern (unit cell) that may be based on a great number of shapes like square loops [8] or holes arranged in a honeycomb order [9]. In this work we explore the integration of CEBs into an FSS formed by a periodic 2-D array of annular square and ring motif. All the optical power coupled to such an integrated structure is delivered to the bolometers in a narrow frequency band which is determined mostly by the bolometer-free FSS. The imaginary part of the effective surface impedance of the integrated network can be tuned out by the substrate thickness which can be more than quarter (or half) of the wavelength, since the well matched layer of the FSS+CEB array suppresses any substrate modes. A single CEB can handle a finite amount of absorbed power before the electron temperature in absorber increases enough to reduce the responsivity of the device. For handling large power loads typical to balloon-borne missions, an array of CEBs was proposed where incident power could be distributed to keep all bolometers running at lower temperatures [10]. This created a problem of efficiently coupling incident radiation equally to all detectors in the array in a way to avoid the overheating of one (or a few) detectors. Also, the balloon-borne experiments mentioned earlier have been designed to use room temperature JFET amplifiers as readout. The impedance of the CEB array needs

Manuscript received August 25, 2014; revised November 17, 2014; accepted November 26, 2014. Date of publication December 18, 2014; date of current version January 14, 2015.

S. Mahashabde and L. S. Kuzmin are with the Department of Microtechnology and Nanoscience, Chalmers University of Technology, 41296, Göteborg, Sweden (email: sumedh@chalmers.se).

A. S. Sobolev is with Kotelnikov Institute of Radio Engineering and Electronics, 125009, Moscow, Russia, and also with the Moscow Institute for Physics and Technology (State University), 141700, Dolgoprudny, Moscow region, Russia.

M. A. Tarasov is with Kotelnikov Institute of Radio Engineering and Electronics, 125009, Mokhovaya st 11/7, Moscow, Russia.

G. E. Tsydynzhapov is with Institute of Solid State Physics RAS, 142432 Chernogolovka, Moscow region, Russia, and also with Terasense Development Labs LLC 2, Chernogolovka city, Moscow region, 142432, Russia.

Color versions of one or more of the figures in this paper are available online at <http://ieeexplore.ieee.org>.

Digital Object Identifier 10.1109/TTHZ.2014.2377247

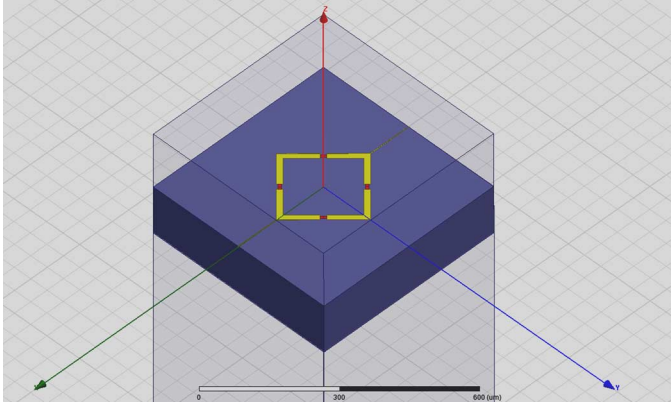


Fig. 1. Layout of a single cell of FSS+CEB simulated in HFSS package. The annular square shape along with connecting lines in X -direction form the FSS. CEBs are integrated in the arms of the square. The top face of the layout is the backshort.

to be matched to the noise impedance of these amplifiers. We believe that these problems can be solved by implementing a combination of FSS with an array of CEBs integrated in it.

II. FSS DESIGN

A. FSS and Integrated CEB Detectors

The CEB is a sensitive direct detector with a nonlinear current–voltage characteristic which is dependent on the electron temperature of the normal metal absorber. The CEBs are connected in a series/parallel network to maximize the voltage response to incident power, while at the same time decreasing the total dynamic resistance of the array to match to the noise impedance of JFET amplifiers. We can use the model from [11] to explain the optical response from the series/parallel array.

We begin the design process by choosing a FSS motif that can conveniently integrate one (or more) CEB detector in it. A simple motif is an annular square in the arms of which CEBs can be placed. To couple the detectors to readout, the array of squares need to have coupling lines carrying dc current. Thus the final form of the repeating motif becomes an annular square with lines connecting in one direction. Using a transmission line model described in the next section, estimates are made of the real and imaginary part of impedances offered by the substrate and a backshort. Next, a proper size of the unit cell needs to be chosen. This depends on the Airy spot due to the telescope optics, number of detectors per unit cell, the required imaginary part of impedance that needs to be compensated by the substrate (from estimates) and the total number of detectors that could be used without increasing the pixel NEP beyond the required limit [3]. In our first design a unit cell size of $522 \mu\text{m} \times 522 \mu\text{m}$ is considered which would allow about 30 unit cells in a circular area of 3 mm diameter. These considerations come from the design of a horn coupling the telescope beam to the pixel. This pixel design is created and simulated in the commercial 3-D electromagnetic simulator HFSS. The HFSS layout is shown in Fig. 1. The unit cell is illuminated with a Floquet excitation with two orthogonal modes. Periodic boundary conditions are applied to the unit cell to simulate an infinite FSS array.

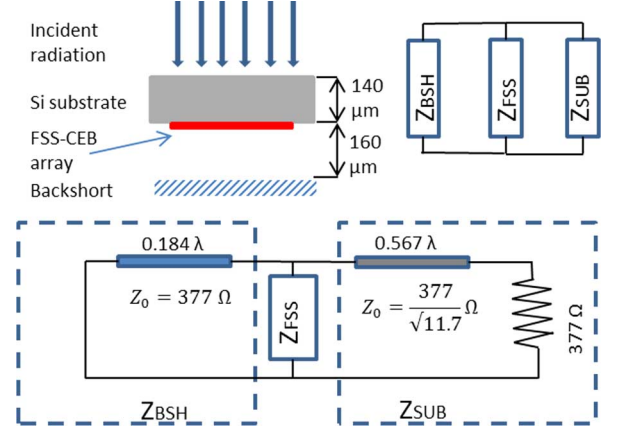


Fig. 2. 1-D transmission line model with values corresponding to a measured sample.

B. Transmission Line Model

The schematic of the device is shown in Fig. 2. Since the substrate modes are efficiently absorbed by the FSS layer, it can be described with a simple one dimensional transmission line equivalent circuit diagram as shown. The FSS layer with integrated bolometers serves as an impedance matched absorber for coupling incident electromagnetic radiation together with the substrate and the backshort. The impedance of the substrate is modelled as a transmission line with a finite electrical length corresponding to its thickness in series with the free space impedance of 377Ω . Similarly, the backshort distance is modelled as a transmission line with an electrical length corresponding to its distance from the FSS. These two impedances are arranged in parallel to the FSS impedance. At resonance, the imaginary part of the FSS surface impedance is tuned out by the substrate and the backshort impedances. Since high frequency currents are excited in the FSS motif, they pass through the matched load (CEB) present in the arms of the motif, cause dissipation of power in the CEB and create a voltage/current response which can then be read out.

C. FSS Tuning

Using the one dimensional model described above, an estimate can be made of the impedance offered by the substrate and the backshort. Initially, a suitable thickness of substrate and a suitable backshort distance is chosen and their impedance calculated using the equation for the input impedance of a transmission line. The transmission line equivalent corresponding to the backshort length can be considered to be lossless and its impedance is equal to

$$Z_{\text{BSH}} = 377 * i * \tan(k_{\text{BSH}} * H_{\text{BSH}}). \quad (1)$$

Here, k_{BSH} is the wavenumber in vacuum and H_{BSH} is the distance to the backshort. Similarly, the impedance offered by the combination of substrate and free space is calculated as

$$Z_{\text{SUB}} = Z_0 * \frac{377 + Z_0 * i * \tan(k_{\text{SUB}} * H_{\text{SUB}})}{Z_0 + 377 * i * \tan(k_{\text{SUB}} * H_{\text{SUB}})} \quad (2)$$

$$Z_0 = \frac{377}{\sqrt{11.7}} \quad (3)$$

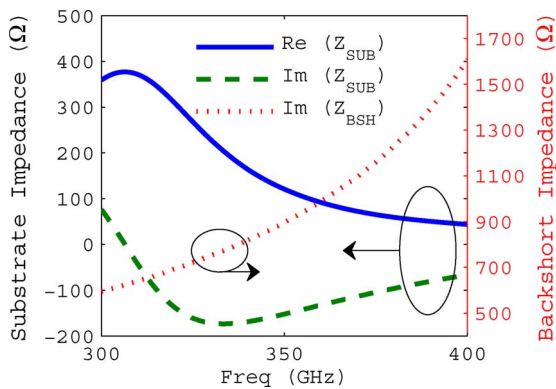


Fig. 3. Estimation of impedance of the silicon substrate and the backshort using the transmission line model.

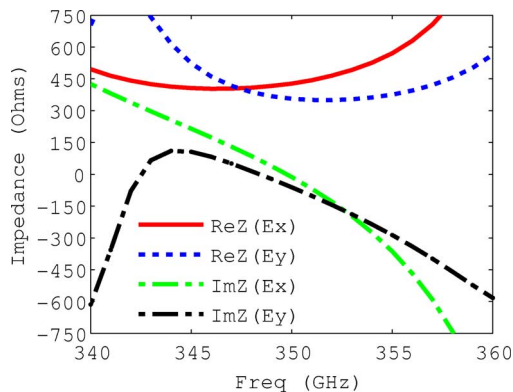


Fig. 4. Impedance of the FSS computed using two orthogonal modes of the Floquet excitation. The difference is due to the presence of connection lines in one direction (X) that increase the inductive part of the impedance.

where k_{SUB} and H_{SUB} are the wavenumber in the substrate and the substrate thickness. The wave impedance in vacuum is taken to be 377Ω and the relative permittivity of Silicon is assumed to be 11.7 in (3).

The impedances are plotted in Fig. 3 for a thickness of Silicon of $140 \mu\text{m}$ and distance to the backshort of $160 \mu\text{m}$. The imaginary part of the impedance of the substrate is capacitive and dominates that of the backshort. Fig. 4 shows the impedance of the FSS. This can be estimated from simulations by moving the reference plane to the FSS surface thus de-embedding out the substrate. Alternately, one can de-embed the substrate out by removing the parallel substrate impedance component calculated using the transmission line model. The simulations need to be done with the FSS illuminated together with the substrate since the calculation then includes the effect of the near fields excited in the substrate. In this region the transmission line model of the substrate impedance is not valid but since the near field zone is smaller than the thickness of the substrate, the model remains a reasonable approximation.

D. Return Loss

The FSS performance is simulated using 3D electromagnetic simulation software HFSS. Since the array is designed for sensing arbitrarily polarized radiation we optimized the

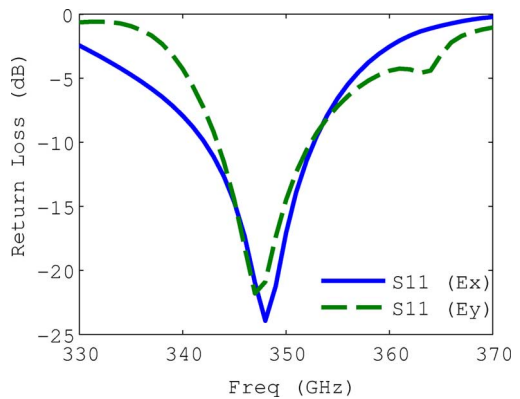


Fig. 5. Return loss computed using two orthogonal modes of the Floquet excitation. The difference is due to difference in imaginary part of the impedance shown in Fig. 4.

reflection loss for the two orthogonal linearly polarized modes of the Floquet port. At high frequency the bolometers are equivalent to a lumped element consisting of a 150Ω resistor connected in series with a 25 fF capacitor [12]. We represent the 4 embedded CEB detectors with ports of the same impedance as the devices and calculate the scattering parameters of the system. The FSS is represented using a lossy gold metal layer. The return loss for both the Floquet modes is shown in Fig. 5. To calculate the delivered power to the detectors, we use the scattering matrix between the Floquet port and the 4 CEB ports (numbered 2–5). We observe that the loss in the gold lines of the FSS is negligible, and the relation $\sum_{n=2}^5 S_{1n}^2 + S_{11}^2 = 1$ is satisfied, where S_{1n} is the power coupled to the n -th detector port from the 1-st mode of the Floquet port (S_{11}). Thus, S_{11} can be used to describe the optical coupling to the detectors while simulating the complete pixel.

The substrate thickness can be used for tuning the resonance frequency of the device. This is possible due to fact that within a reasonable thickness range of the substrate, the impedance is capacitive which can compensate the inductive impedance of the FSS. In Fig. 6, the variation of the resonance frequency with the substrate thickness is simulated and plotted for one of the Floquet modes. It can be noted that spurious resonances are visible higher than the main resonance frequency with very large quality factor. We think that these resonances can be explained by the Wood anomaly found in diffraction gratings [13].

E. DC Model

The DC model of the detector involves solving the heat balance equation where the different effects that can heat up the electron system of the normal absorber are balanced against the effects that cool the system, with the electron temperature being the affected variable. The various heating terms are incident power, power transferred by the bias current, Joule dissipation due to the bias current, etc. The electron–phonon coupling in the normal metal and the electron tunneling across the NIS junction contribute to the cooling of the electron system. The basic heat balance equation is

$$2P_N + 2\beta P_S + \Sigma \Lambda (T_e^5 - T_{\text{ph}}^5) + I^2 R_a + \frac{(P_0 + \delta P)}{M} = 0. \quad (4)$$

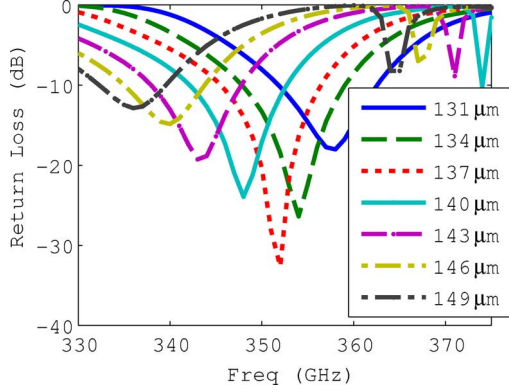


Fig. 6. Dependence of resonance frequency on the thickness of silicon substrate as noted in the legend.

Here, P_N is the power transferred by the bias current, P_S is the power deposited in the superconducting electrode, β is a parameter [14] that refers to the fraction of power deposited in the superconducting electrode that returns back to the normal absorber. $\Sigma\Lambda(T_e^5 - T_{ph}^5)$ is the heat flow from electron to phonon subsystems in the absorber, Σ is the electron-phonon coupling constant which is material and temperature dependent, Λ is the volume of the normal absorber, T_e is the electron temperature of the absorber and T_{ph} is the bath temperature. I is the bias current, R_a is the resistance of the absorber. P_0 is the background power on the pixel in steady state while δP is the incident signal power. M is the total number of detectors in the array. The current through a SIN junction can be expressed as [15], [16]

$$I = \frac{1}{eR_N} \int_{-\infty}^{\infty} \nu(E) (f_N(E - eV) - f_S(E)) dE. \quad (5)$$

Here e is the electron charge, R_N is the normal resistance of the junction and V is the voltage across the junction. $\nu(E)$ is the Dynes density of states [17] in the superconducting electrode and $f_N(E)$ is the Fermi-Dirac distribution for the normal metal. $f_S(E)$ is the Fermi-Dirac distribution of quasi-particles in the superconductor and in general it will be different from $f_N(E)$ since they can have different electron temperatures.

The tunneling electrons in the SIN junction will carry with them some power, P_N can be calculated by removing one e in (5) and replace it with $eV - E$ which is the energy deposited in the normal metal from one tunneling event. Doing this we obtain [15]

$$P_N = \frac{1}{e^2 R_N} \int_{-\infty}^{\infty} (eV - E) \nu(E) (f_N(E - eV) - f_S(E)) dE. \quad (6)$$

It is possible for P_N to be negative and this is the electron cooling effect. From energy conservation we conclude that the power dissipated in the superconductor is

$$P_S = IV - P_N \quad (7)$$

$$S_v = -2 \frac{\frac{\partial I}{\partial T} / \frac{\partial I}{\partial V}}{5\Sigma\Lambda T_e^4 + 2 * \left(\frac{\partial P}{\partial T} - \left(\frac{\partial I}{\partial T} / \frac{\partial I}{\partial V} \right) * \frac{\partial P}{\partial V} \right)}. \quad (8)$$

S_v is the responsivity of the CEB in current biased mode. P is the power transferred by the bias current, essentially P_N . $\partial I / \partial T$ and $\partial I / \partial V$ are the partial derivatives of the current with

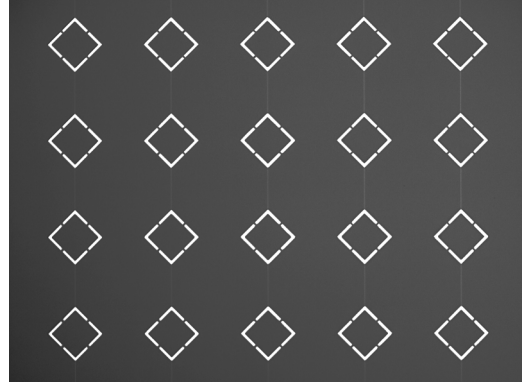


Fig. 7. An optical picture of the device fabricated on Silicon substrate. The gold squares and connecting lines can be seen. The bolometers are integrated in the small gaps in the arms of the squares. Size of one arm of the square is about $200 \mu\text{m}$ while the typical size of the bolometers is about $2 \mu\text{m}$.

respect to temperature and voltage. $\partial P / \partial T$ and $\partial P / \partial V$ is the partial derivative of the power with respect to the normal metal electron temperature and voltage [16]. The factor 2 comes from the fact that there are two NIS junctions in the CEB device. This value of the responsivity can be used to fit the experimental data to estimate the power absorbed in the detector.

III. EXPERIMENT

The FSS integrated CEBs were fabricated on a silicon substrate. The fabrication process consists of multiple lithography layers. The most important part is the trimming of the Silicon substrate to the required thickness. We use the Bosch Process to thin down the Silicon using SF_6 gas plasma. We stop the plasma process at the required etch depth. The next layer involves the lithography of the gold FSS pattern. The final layer involves the exposure and deposition of the CEB devices. The normal metal absorber is a thin (10 nm) Aluminum film whose superconductivity is suppressed by ferromagnetic impurities (Cr/Fe). The NIS tunnel barrier is created in-situ by oxidation of the Aluminum normal metal. Finally, superconducting Aluminum counter electrodes of about 70 nm thickness each are deposited and unwanted metal is lifted off, similar to [18]. An optical image of a finished sample is shown in Fig. 7. Measured parameters of the fabricated sample were: $R_n = 1 \text{ k}\Omega/\text{junction}$, $R_a = 150 \Omega$.

The experimental setup consists of illuminating the sample with blackbody radiation from a cold blackbody source. The sample together with band defining quasi-optical filters is mounted on the mixing chamber of a dilution cryostat. Additional filters to cut off infrared radiation are also mounted on the sample holder. The sample holder faces a cold blackbody mounted on the 2.7 K stage of the cryostat with low thermal conductivity legs to ensure that the blackbody does not heat up other parts of the cryostat by conduction heating. The blackbody temperature can be varied as desired. The CEB array is current biased and commercial JFET amplifiers are used to read out the voltage response of the device. This is shown in Fig. 8.

As shown in this figure, a strong voltage response is obtained to radiation from a blackbody heated up to temperatures of 7 K. This data was taken with the bath temperature of 185 mK.

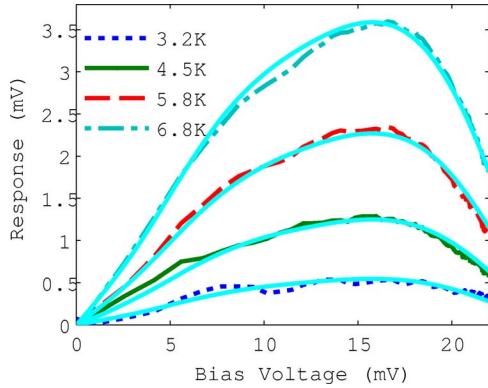


Fig. 8. Voltage response of the array to blackbody radiation plotted against voltage across the array at temperatures shown in the legend. The bath temperature for this measurement was 185 mK. The solid lines indicate data fits using (8). (bottom to top) The absorbed power is 0.24, 0.5, 1, and 1.6 pW, respectively.

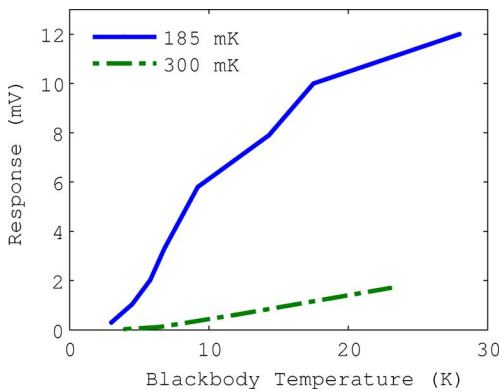


Fig. 9. Comparison of optical response at two different bath temperatures.

Similar experiment was conducted with the bath temperature of 300 mK. The maximum response obtained at these two bath temperatures are plotted in Fig. 9. It can be noticed that the responsivity at 300 mK is about 5–7 times lower than at 185 mK. The estimated responsivity from data fits at 185 mK is greater than 2×10^9 V/W and about 3×10^8 V/W at 300 mK.

The response of the FSS integrated detectors to radiation from a backward wave oscillator (BWO) is shown in Fig. 10. The top panel shows the response of detectors embedded in the square motif and the bottom panel shows the response of detectors embedded in the ring shaped motif. The simulation results for coupling are also shown. The experiment consisted of a BWO radiating through the optical windows of the cryostat through a chopper. A pyroelectric detector measured the BWO power. The optical response and the pyroelectric detector response were measured with lock-in amplifiers. In experiments we observe the effect of multiple reflections inside the cryostat which can appear as discontinuities in the response (especially seen at 330 GHz in Fig. 10 upper panel). We are in the process of optimizing the measurement setup to reduce the effect of such reflections. The peak of the optical response is shifted towards longer wavelengths for the square motif FSS. We believe this is due to etching of the substrate to a larger thickness than intended.

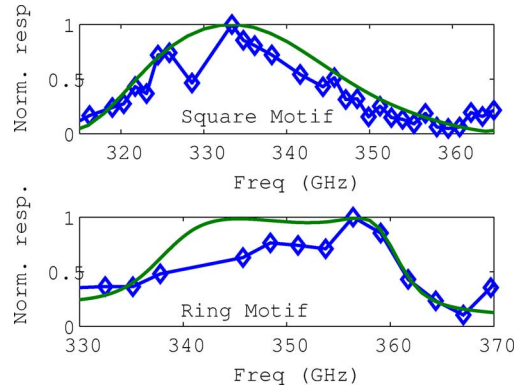


Fig. 10. Measured response of FSS integrated detectors to radiation from a BWO. The solid lines are simulations while the connected diamonds are measurements.

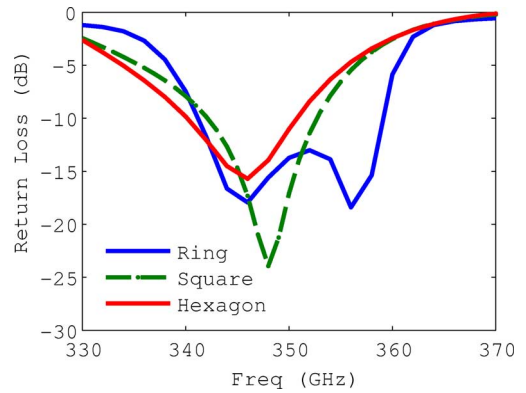


Fig. 11. A comparison of three different shapes of the FSS motif – a ring, an annular square and an annular hexagon. The simulations were made for substrate thickness of $140 \mu\text{m}$ and backshort distance of $160 \mu\text{m}$. The bolometer impedance is also kept the same (100Ω resistance and 25 fF capacitance).

IV. DISCUSSION

As discussed earlier, the FSS integrated CEB array solution was developed to ensure an efficient distributed coupling system with an array of bolometers. Since the FSS can be designed with any possible repeating motifs, a study was made to compare between different shapes of the motif with regards to the impedance matching properties. Three shapes were chosen—a ring, an annular square described earlier and an annular hexagon. The topologies of the motifs remain the same—an annular shape with two connecting lines for dc bias and 4 bolometers embedded in the arms. The matching chiefly depends on complex part of the impedance of the FSS and the substrate, and how well they can compensate each other. Fig. 11 shows the comparison of the return loss for one of modes of the Floquet excitation. The -3 dB bandwidth for all 3 shapes is comparable, but the ring shape is better when comparing the -10 dB bandwidths. Overall, the choice of shapes depend on the presence (and absence) of possible places for exciting surface resonances [13]. A square and a hexagonal motif have sharp corners that can give rise to such unwanted resonances while a ring shape is free of such “sharp corners.” In general the FSS based detectors have a limited bandwidth between 5%–10% at the frequency of interest. While this can be a limiting factor for some balloon missions, especially LSPE

[4] which needs up to 25%, we are working towards increasing the bandwidth of the device. This could involve wider elements or different sized unit cells arranged next to each other but tuned to slightly lower and slightly higher center frequency each.

The measured data was fitted to the CEB model using (8) and absorbed power was estimated. The fitting parameters are $\Sigma = 2.1 * 10^9 \text{ W}/\mu\text{m}^3 \text{ K}^{5.4}$, energy gap of superconductor (Δ) = 195 μeV , $\beta = 0.13$, $P_0 = 5 \text{ fW}$. It has been shown that the electron phonon decoupling (T_e^n , T_{ph}^n , $5 < n < 6$) increases as the bath temperature is lowered. The value of electron-phonon coupling constant (Σ) used for fitting is comparable to the one reported in [19] for normal metals fabricated from Aluminum with its superconductivity suppressed by ferromagnetic impurities. The high value of β is probably due to very small volume of superconducting electrodes in these series of prototypes. Due to power deposited in electrodes (P_S), the temperature of quasi-particles in the superconductor increases. This is taken into account while calculating the data fits in Fig. 8 contrary to the classical CEB model [16] where the temperature of quasi-particles in electrodes was assumed to be equal to bath temperature. Quasi-particles in aluminum have a long lifetime and in a small volume are more liable to interact with phonons and deposit some power back into the normal metal absorber which increases electron temperature in absorber and decreases cooling power.

V. CONCLUSION

We have designed, fabricated and measured a CEB array integrated in an FSS. We have shown that it is possible to design such an array with unit cell spacing larger than half of the wavelength in the substrate thus decreasing the number of devices required to fill the Airy spot on the focal plane and lowering the NEP. Furthermore, the substrate thickness is shown to tune out the surface impedance of the FSS-based array and can also be used as a frequency tuning element. Cryogenic measurements with a cold blackbody show very strong optical response, comparable to previously reported CEB-based architectures in this frequency range. We also explored the possibility of using different shaped motifs of the FSS to improve the bandwidth of this device.

ACKNOWLEDGMENT

The authors would like to acknowledge V. S. Edelman for making low temperature measurements.

REFERENCES

- [1] L. Kuzmin, "Optimization of the hot-electron bolometer and a cascade quasiparticle amplifier for space astronomy," in *Int. Workshop on Superconducting Nano-Electron. Devices*, 2002, pp. 145–154.
- [2] B. Crill *et al.*, "Boomerang: A balloon-borne millimeter-wave telescope and total power receiver for mapping anisotropy in the cosmic microwave background," *Astrophys. J. Supplement Series*, vol. 148, no. 2, p. 527, 2003.
- [3] F. Nati *et al.*, "The OLIMPO experiment," *New Astronomy Rev.*, vol. 51, no. 3, pp. 385–389, 2007.
- [4] S. Aiola *et al.*, "The Large-Scale Polarization Explorer (LSPE)," in *SPIE Astronomical Telescopes+ Instrument.*, 2012, p. 84467A.
- [5] M. Salatino, P. de Bernardis, L. Kuzmin, S. Mahashabde, and S. Masi, "Sensitivity to cosmic rays of cold electron bolometers for space applications," *J. Low Temp. Phys.*, pp. 1–8, 2014.
- [6] G. M. Rebeiz, "Millimeter-wave and terahertz integrated circuit antennas," *Proc. IEEE*, vol. 80, no. 11, pp. 1748–1770, Nov. 1992.
- [7] S. Doyle, J. Naylor, P. Mauskopf, A. Porch, S. Withington, D. Goldie, D. M. Glowacka, J. J. Baselmans, S. J. Yates, and H. Hoevers, "Lumped element kinetic inductance detectors for far-infrared astronomy," *SPIE Astronomical Telescopes+ Instrumentation*, p. 70200T, 2008.
- [8] Z. Shen *et al.*, "Frequency selective surface notch filter for use in a millimeter wave imaging system," in *IEEE Antennas Propag. Soc. Int. Symp.*, 2006, pp. 4191–4194.
- [9] C. Winnewisser, F. Lewen, J. Weinzierl, and H. Helm, "Transmission features of frequency-selective components in the far infrared determined by terahertz time-domain spectroscopy," *Appl. Opt.*, vol. 38, no. 18, pp. 3961–3967, 1999.
- [10] L. Kuzmin, "An array of cold-electron bolometers with SIN tunnel junctions and JFET readout for cosmology instruments," in *J. Phys.: Conf. Series*, 2008, vol. 97, p. 012310, 1.
- [11] L. Kuzmin, "Distributed antenna-coupled cold-electron bolometers for focal plane antenna," in *Proc. ISSIT*, 2008, pp. 154–158.
- [12] L. S. Kuzmin, "On the concept of a hot-electron microbolometer with capacitive coupling to the antenna," *Phys. B: Condens. Matter*, vol. 284, pp. 2129–2130, 2000.
- [13] R. Wood, "Anomalous diffraction gratings," *Physical Rev.*, vol. 48, no. 12, p. 928, 1935.
- [14] P. Fisher, J. Ullom, and M. Nahum, "High-power on-chip microrefrigerator based on a normal-metal/insulator/superconductor tunnel junction," *Appl. Phys. Lett.*, vol. 74, no. 18, pp. 2705–2707, 1999.
- [15] G. C. O'Neil, *Improving NIS Tunnel Junction Refrigerators Modeling, Materials, and Traps*, 2011.
- [16] D. Golubev and L. Kuzmin, "Nonequilibrium theory of a hot-electron bolometer with normal metal-insulator-superconductor tunnel junction," *J. Appl. Phys.*, vol. 89, no. 11, pp. 6464–6472, 2001.
- [17] R. Dynes, V. Narayanamurti, and J. P. Garno, "Direct measurement of quasiparticle-lifetime broadening in a strong-coupled superconductor," *Phys. Rev. Lett.*, vol. 41, no. 21, pp. 1509–1512, 1978.
- [18] M. Tarasov, L. Kuzmin, and N. Kaurova, "Thin multilayer aluminum structures for superconducting devices," *Instruments and Experimental Techn.*, vol. 52, no. 6, pp. 877–881, 2009.
- [19] J. M. Underwood, P. J. Lowell, G. C. O'Neil, and J. N. Ullom, "Insensitivity of sub-kelvin electron-phonon coupling to substrate properties," *Phys. Rev. Lett.*, vol. 107, no. 25, 2011, Art ID. 255504.



Sumedh Mahashabde was born in India in 1985. He received his B.E. degree from Mumbai University, Mumbai, India, in 2007, the M.Sc. degree from Chalmers University of Technology, Gothenburg, Sweden, in 2010, and is currently working toward the Ph.D. degree in physics at the same university. His research interests include terahertz bolometers, superconducting tunnel junctions and Graphene.



Alexander S. Sobolev received the M.Sc. and Ph.D. degrees from Moscow Institute of Physics and Technology (State University), Moscow, Russia, in 2003 and 2006, respectively.

His Master and Ph.D. research was related to the development of the fully superconducting integrated receiver for the instrument TELIS. During this work, he made a number of research visits to the Technical University of Denmark (DTU) and Netherlands Institute for Space Research (SRON). At present, he is a Senior Research Fellow at Kotel'nikov Institute of Radio Engineering and Electronics (Russian Academy of Sciences), Moscow, Russia. His current research interests include long Josephson junctions, sub-mm detectors and heterodyne receivers, integrated superconducting circuits, sub-mm antennas and focal plane detectors array.



Mikhail A. Tarasov received the Master's degree from M. Lomonosov Moscow State University in 1977, and the Ph.D. and the Doctor of Sciences (Habilitation) degrees from V. Kotel'nikov Institute of Radio Engineering and Electronics of the Russian Academy of Sciences in 1983 and 1997, respectively.

Since 1977, he has been with V. Kotel'nikov Institute, Moscow, Russia, where he is currently a Principal Investigator. For the last 20 years, he has been spending up to six months every year with Chalmers University of Technology, Gothenburg, Sweden, collaborating in development of SIS mixers, Josephson detectors, SQUID amplifiers, and cold electron bolometers. The list of his publications includes over 200 papers in scientific journals and proceedings of international conferences. His research interests are mainly in superconducting electronics, low temperature physics, microwave spectroscopy, and noise in superconducting devices.



Gombo E. Tsydynzhapov received the M.Sc. degree from the Moscow Institute for Physics and Technology in 1996, and the Ph.D. degree from the Institute for Solid State Physics of RAS in 2000. His Ph.D. thesis and subsequent work was related to high-temperature superconductivity and strongly correlated electron systems. Later, his research interest shifted to detection of sub-terahertz radiation and sub-terahertz imaging.

Currently, he is a research scientist with Institute for Solid State Physics Russia and with Terasense Development Labs LLC, Chernogolovka city, Russia.



Leonid S. Kuzmin was born in Moscow, Russia, in 1946. He received the Ph.D. degree in physics (Degree of Candidate of Science in Physics and Mathematics) from Moscow State University, Moscow, Russia, in 1977, with the thesis topic "Non-degenerate single-frequency parametric amplification using Josephson junctions with self-pumping" defended in 1997 and "Correlated Tunnelling of Electrons and Cooper Pairs in Ultrasmall Tunnel Junctions."

In 2000, he was a Docent with Chalmers/Göteborg University. Since 2009, he has been a Professor with Chalmers University of Technology, Gothenburg, Sweden. He is the Chairman of 13 international workshops and three international schools for young scientists with a general title "From Andreev Reflection to the Earliest Universe." He has authored more than 200 publications (including 114 in referred journals; citation index: 1305, h-index: 19, average citations per item: 11.45).